Journal of Catalysis **183,** 182–195 (1999)
Article ID jcat.1999.2412, available online at http://www.idealibrary.com on IDEAL®

Solid-State NMR Investigation of Promoted Silver Catalysts

Eric Hughes,* Jeff M. Koons,* Jianxin Wang,*,[1] and Paul D. Ellis†,[2,3]

*Department of Chemistry and Biochemistry, University of South Carolina, Columbia, South Carolina 20208; and †Environmental Molecular Sciences Laboratory, Pacific Northwest National Laboratory, Battelle Boulevard, P.O. Box 999, Richland, Washington 99352

Received May 20, 1998; revised November 17, 1998; accepted January 5, 1999

The effects of cesium promoters on silver catalysts, supported by γ-alumina, were studied by adsorbing mono- or dilabeled [^{13}C]ethylene onto the catalysts and performing low-temperature (70 K) solid-state ^{13}C NMR measurements on the ethylene. Selective isotopic enrichment was used to investigate the electronic environment present in and around the ethylene molecule as a function of promoter concentration. Changes in the spectroscopic parameters describing the ethylene lineshapes were extracted using a nonlinear least-squares procedure. These parameters were then used to determine the structure of the ethylene molecule on the surface and to probe the changes induced by adding cesium promoters. Similarly, the state of cesium in the catalyst system was investigated by spin-echo double-resonance spectroscopy and scanning electron microscopy X-ray fluorescence methods. The results imply that the form of cesium is not that of an oxide but, in all probability, reflect those of a cation–anion pair.

INTRODUCTION

Ethylene oxide (EO) has been prepared commercially for more than 50 years by the reaction of oxygen or oxygenated gases with ethylene in the presence of silver catalysts (1, 2). As early as 1936 it was realized that by incorporating small amounts of alkali salts into impregnation solutions for silver catalyst preparation (often referred to as "alkali salt promotion" or "promotion") and enhancement in the rate of ethylene oxide production could be achieved (3, 4). Since that time a significant amount of research has been focused on determining the role of the alkali metal in the epoxidation reaction to improve the catalyst's efficiency in producing ethylene oxide (5–9). In contrast less thought has been given to nature of the anion on the surface and its potential role in promotion (10).

As with most supported metal catalyst systems, much of the insight into the effects of promoters in the EO process have been obtained by analogy with the ultrahigh vacuum (UHV), 10^{-7}–10^{-9} Torr, experiments (11–14). These experiments have been used to investigate the interactions between a single crystal of the transition metal surface and coadsorbed (i) alkali metals and (ii) certain reactive gases. From such studies, it has been shown that the workfunction of the substrate metal decreases linearly for small coverage of alkali metal. Subsequently a minimum is reached and then the workfunction starts to increase on further coverage to a characteristic value due to an overlayer (15). Furthermore, it has been observed that neutral small molecules coadsorbed with the alkali show an increased binding affinity to the transition metal substrate (16). This increased affinity of the neutral molecules has been explained by the action of the alkali atoms in lowering the workfunction of the substrate metal and it has been postulated that this action can be used to explain the alkali promoter effect in catalysts.

This characteristic of alkali metal adsorption onto a transition metal surface can be explained by using the model of Lang (17) for chemisorption to metal surfaces by neutral adatoms. This model depicts the metal surface as being continuous, with a dipole existing above and below the surface. Below the surface there exists a positive charge, and above, a negative charge that extends into space. In the process of removing an electron from the Fermi level of the surface [the highest (extended) molecular orbital of the surface metal atoms] work must be performed against the dipole. The amount of work required to accomplish this defines the workfunction in its simplest form. Assuming this model, consider an ethylene molecule chemisorbed to the surface through its π electrons. For backbonding (from the metal surface to the olefin) to take place the metal conduction electrons have to overcome the surface dipole and transfer from silver to ethylene π^* orbitals. The addition of an electropositive polarizable alkali atom will reduce the local dipole and thereby decrease the workfunction and increase the affinity for the silver to backbond to the π^* orbitals of ethylene. As a result of this backbonding,

[1] Union Carbide Fellow.

[2] A brief summary of a portion of this work appeared in Maciel, G. E., and Ellis, P. D., NMR techniques in catalysis, *in* "NMR Characterization of Silica and Alumina Surfaces" (A. T. Bell and A. Pines, Eds.), pp. 231–309. Marcel Dekker, New York, 1994.

[3] To whom correspondence should be addressed. Fax: 509 376–2303. E-mail: pd_ellis@pnl.gov.

0021-9517/99 $30.00

there should be a corresponding increase in the value of r_{CC}.

Under oxidizing conditions that produce ethylene oxide, Campbell found that cesium atoms formed an oxide species ($Cs^+O_3^-$ was proposed) on the surface of the Ag(111) crystal (18). Campbell attributed the role of this cesium oxide as a site blocker, via an ensemble effect, stopping isomerization of the ethylene oxide and the subsequent secondary combustion. Since the cesium is added to the real catalyst as a salt, it is reasonable to propose that it is present as a cation. Moreover, site blockers in the form of organic chlorides were one of the first recognized promoters of this reaction (1, 2). Carter and Goddard (22), after performing *ab initio* studies, have proposed that the cesium oxide cluster observed experimentally sits on top of the 4-coordinate trough sites of the Ag(110) surface with the oxygen between the cesium and silver. They propose that the action of this species is to direct the ethylene to the silver.

What is required is experimental evidence from systems that more closely resemble the industrial process in terms of promoter speciation. This would allow one to link the important results and models of the UHV work more directly to the catalytic process. To this end, we have used solid-state NMR techniques to investigate catalysts that more closely resemble industrial materials (in both heterogeneity and promoter characteristics) than the single-crystal surfaces used in the UHV experiments (13–16, 18). Recently, solid-state NMR experiments have been reported that show that investigations of catalyst surfaces are possible and that detailed structural information about changes in the electronic structure of adsorbates can be obtained. In particular, Chin and Ellis (20) have shown that ethylene adsorbed on a high-surface-area γ-alumina-supported silver catalyst can be studied by ^{13}C solid-state NMR. Their results indicated a symmetric bonding of the ethylene with respect to the silver surface (as seen by a single resonance at room temperature for both carbons under magic-angle spinning conditions). Furthermore, they showed that the isotropic chemical shift changed from 123 ppm for ethylene to 108 ppm for ethylene adsorbed to a silver catalyst at room temperature. They concluded that this change was indicative of an olefin ligand bound to a metal surface via a π-bond interaction given that the isotropic chemical shift for CH_2 in $[Ag(CH_2{=}CHCH_3)_2]^+$ is 109 ppm, which is known to have a π-bond interaction with silver (21). In addition, Chin and Ellis saw no evidence of a chemical shift anisotropy (CSA) powder pattern lineshape for ethylene at room temperature, indicating a fast, nearly isotropic molecular motion for the surface-adsorbed ethylene. This result was predicted by Carter and Goddard who, based on *ab initio* calculations, suggested that there should be no barrier to rotation (or translation) at room temperature (22). However, on decreasing the temperature to 100 K, a CSA powder pattern was observed, having the following principal elements: $\delta_{11} = 192$ ppm, $\delta_{22} = 117$ ppm, $\delta_{33} = 12$ ppm. This result manifested a marked deviation in the δ_{11} element relative to the measurements made by Zilm and Grant for ethylene diluted in an argon matrix (23). Parallel to the efforts of Zilm and Grant, Chin and Ellis, in their studies involving dilabeled ethylene at 100 K, demonstrated that it was possible to extract the orientation of the chemical shift tensor and the bond distance from the ethylene adsorbed to the silver surface. They found, within the limitations of their analysis, that the orientation of the chemical shift tensor relative to the molecular frame was the same as in Zilm and Grant's work, with the δ_{33} element perpendicular to the plane of the molecule, the δ_{22} element parallel to the carbon–carbon bond vector, and the δ_{11} element perpendicular to both. Therefore, the marked change in the δ_{11} element was assigned to an interaction between the silver 4*d* orbitals and a virtual antibonding π^* orbital on ethylene. The change in the δ_{11} element for this system indicated a perturbation in the electron density in the π orbitals above and below the plane of ethylene.

Wang and Ellis (24) have expanded this work to include a study of promoter effects by incorporating alkali salts into the silver catalyst by the method of Nielsen and La Rochelle (25). Although they studied rubidium, potassium, and cesium, most of the detailed investigations were performed on catalysts prepared with $CsNO_3$. The first observation they made was that the ethylene was bound more tightly to the silver surface as the amount of cesium promoter was increased. This was evident in the broadening of the single resonance in the room temperature magic-angle spinning experiments performed on promoted silver catalysts consisting of 0, 5, 10, 14, 17, and 30% by weight Cs^+ relative to the weight of silver on the catalyst. In addition, by following the changes in static CSA lineshape as a function of temperature, a model for the motion of ethylene on the catalyst surface was derived. The experiments supported a motional model that consisted of rotation of the ethylene about the axis perpendicular to the plane of the molecule. Further studies of monolabeled [^{13}C]ethylene reflected a change in the isotropic chemical shift from 107 to 100 ppm; i.e., the carbons were becoming more shielded as a function of increasing cesium concentration. This, again, indicated increasing strength in the interaction between the π system of the ethylene and the silver metal. In addition, they observed a systematic change in the δ_{22} and δ_{33} elements of the chemical shift tensor as a function of increasing cesium concentration. They tentatively attributed these differences to changes in the electron density in the plane of the ethylene molecule. Although this assumed the orientation of the chemical shift in the molecular frame did not change on going from the argon matrix to the silver catalyst, preliminary dipolar spectra showed relatively small changes in the orientation of the shift tensor along with

an increase in the bond distance as a function of cesium loading. To date, these three aspects of the [^{13}C]ethylene data—the broadening of the room temperature spectra, the change in the isotropic shift to higher shielding, and the apparent increase in carbon–carbon bond length in the low-temperature studies—would suggest that the cesium promoter, even in the form of a cation, is decreasing the workfunction of the silver surface, increasing the affinity of the ethylene toward it. Indeed, one could envisage cesium ions still being able to lower the workfunction of the silver if it were present on the surface as a polarizable cation–anion pair which could reduce the electrostatic potential near the adsorption site in a manner similar to that of the cesium adatoms on a metal surface in the UHV experiments. One would assume that the properties of this cation–anion pair and its ability to affect the workfunction of the surface metal, would be highly dependent on the anion.

In the present work we have attempted a more detailed quantitative study of the effects of increasing amounts of cesium promoter on the electronic structure of ethylene via NMR lineshape analysis. Through suppression of the chemical shift interaction we have measured directly the ^{13}C homonuclear dipolar coupling in dilabeled ethylene as a function of cesium loading. This has allowed complete analysis of the magnitude of the chemical shift tensor and its orientation with respect to the molecular frame of ethylene as a function of cesium loading.

Of major importance to understanding the promotion effects of alkali metals would be obtaining experimental evidence about the location of the alkali promoter on the catalyst and its chemical speciation. Since the systems used in this study are comparable to industrial catalysts, such direct experimental evidence would help unify the UHV experimental work and the models put forward with real-world systems. To this end we have measured the chemical shift of the cesium, prepared from various salts, to determine the anion present after the calcination process. Also, the solid-state NMR experiment is adept at determining local structure in disordered systems by using the direct dipolar interaction between like and unlike nuclear spins. We have attempted to probe the local environment of the ethylene molecules for evidence of cesium. Spin-echo double-resonance (SEDOR) NMR experiments (26) between ^{133}Cs cesium and the protons on the ethylene have been performed to observe evidence of through-space heteronuclear dipolar couplings. Such an interaction would be observed if the cesium is on the surface of the silver and close to the binding site of the ethylene. With such positive experimental evidence, one would be able to put forward an "equilibrium" model for the interaction of the cesium with the ethylene on a silver catalyst built on the foundations of the UHV studies and proposed models.

EXPERIMENTAL

Catalyst Preparation

Silver nitrate (99.99%), potassium oxalate monohydrate (99%), ethanolamine (99%), and ethylenediamine (99%) were purchased from the Aldrich Chemical Company. γ-Alumina (No. SA 6173, 220 m^2/g) was obtained from Norton Chemical Products Division. $^{13}CH_2CH_2$ (ca. 99.0% atom) was purchased from Isotec (Miamiburg, OH) and $^{13}CH_2{}^{13}CH_2$ (ca. 99.3% atom) was obtained from MSD Isotopes (Rahway, NJ). D_2O (ca. 99.9% atom) was also purchased from Isotec.

Preparation of the γ-alumina/silver catalysts used in this work was similar to the method of Nielsen and La Rochelle (25). A 2.55-g sample of γ-alumina pellets was placed in a 10-ml pear-shaped flask fitted with a stopcock and rubber syringe input septum. The system was evacuated down to 0.1 Torr for 1 h prior to adding the silver solution. Silver oxalate was produced by mixing 25 ml of 0.01 M $AgNO_3$ solution and 25 ml of 0.02 M $K_2C_2O_4$. This composition represents a fourfold excess of silver with respect to a 10 wt% coverage. The white precipitate was washed until the UV–vis absorbance of KNO_3 (302.5–305 nm) was not detectable in the filtrate (27). KNO_3 was not detectable after the precipitate was washed with 250 ml of deionized water. The precipitate was subsequently dried in a 100°C oven until the silver oxalate flaked from the filter paper. For non-alkali-promoted silver catalysts, the silver oxalate was added to a solubilizing solution containing 3.0 ml deionized water and 700 μl ethylenediamine. Otherwise, the desired cesium salt was added to the solubilizing solution prior to the addition of silver oxalate. The cesium salt was not added in excess and was based on the weight percentage of silver metal deposited, e.g., 10%. The amount of cesium nitrate used was 0.0738 and 0.1387 g for the 14 and 26% cesium samples, respectively. In all cases, the solution was stirred with a glass stirring rod for several minutes; when the precipitate dissolved, the solution color was light amber. After dissolution, 400 μl of ethanolamine was added and the solution usually turned light brown. The silver/(cesium) solution was aspirated into a syringe through a 20-gauge hypodermic needle and injected through the rubber septum. The stopcock was then closed and the system was left for 2 h. After reaction, the impregnated alumina was separated from the liquid by decantation and filtration and was allowed to dry in the hood for 1–2 days. Within several hours of drying, the impregnated alumina pellets appeared light purple. After the drying period, the alumina-supported silver catalyst was subsequently ground into a fine powder and placed in a Pyrex tube and heated at 160°C for at least 12 h. Compressed air was continuously flowing during this heating cycle. After the 160°C heating step, the powder went from a light yellow color to black. The next step consisted of reducing the supported silver by a 4-h heating step at 360°C.

The catalyst changed from black to a whitish gray, indicating some metallic silver was produced.

When deuterated surfaces were required, labile protons were exchanged for deuterium at the last step of the catalyst preparation. In all cases, approximately 1 g of the catalyst was taken after the 360°C heating step and placed in a round-bottom flask fitted with a ground-glass stopcock and a vacuum connection. D_2O 5–10 ml was added to the flask and the system was evacuated. The catalyst was refluxed in D_2O until dryness (usually about 8 h). The catalyst did not undergo any visible color change during this process. After the reaction was completed, the evacuated flask was transferred to an inert N_2 atmosphere glove box (Vacuum Atmospheres, Hawthorne CA) where the sample was removed from the reaction vessel and transferred into a glass heating tube used for further catalyst treatment and ethylene adsorption.

Scanning Electron Microscopy X-ray Fluorescence

Elemental analysis of selected air-activated silver catalysts was performed by Robertson Microlit (New Jersey) by digesting the catalyst sample and determining the composition by atomic adsorption. Routine detection of silver and cesium was performed at Pacific Northwest National Laboratory (PNNL) by using a JEOL JSM-25S III scanning electron microscope equipped with a Tracor Northern TN 2000 X-ray fluorescence accessory (SEM-XF). In this method, silver catalyst powder was deposited on a stainless-steel die with double-sided tape. A palladium–gold alloy was sputtered onto the surface by means of an evacuated Technics Hummer V sputterer. The sample was then examined by scanning electron microscopy at a potential difference of 20 kV. In all cases, the electron beam was focused on a globular silver deposit. X-ray fluorescence spectra were accumulated for 100 s and analyzed by Tracor Northern's Standardless Semi-Quantitative Analysis software FlexTran. A total of five measurements on the surface were made and the average value was taken to be representative. We found the results of the X-ray fluorescence to agree with the atomic adsorption determination for silver and cesium within 5% in most cases.

Diffuse Reflectance FTIR

Catalyst samples were also characterized using diffuse reflectance infrared spectroscopy. In these experiments, 1.0 mg of catalyst was taken at various stages of deuteration, and was diluted with 1.0 mg of KBr and pulverized. A Nicolet Magna 750 FTIR spectrometer (Nicolet Analytical Instruments) purged with dry nitrogen and equipped with a wide-band liquid nitrogen-cooled mercury–cadmium telluride detector and a "praying mantis"-type diffuse reflectance accessory (Harrick Scientific Corp.) were used to make all measurements. Infrared spectra were acquired at a mirror velocity of 1.626 cm/s and signal averaging was performed for 100 scans. Measurements are reported in Kubelka–Munk (KM) units which express the reflectance (R) of the sample divided by the reflectance of the standard according to $\mathrm{KM} = (1 - R)^2/2R$.

Sample Preparation for NMR Experiments

Prior to the adsorption of ethylene, a 500- to 800-mg catalyst sample was placed in a Pyrex glass vacuum tube and heated at 270°C at 5×10^{-6} to 10^{-5} Torr for 4 h. After heating, the sample changed from whitish gray to gray. The sample was typically left to cool on the vacuum line at 5×10^{-6} to 10^{-5} Torr for 2 to 8 h. After that, a measured amount of ethylene was allowed to enter the tube containing the catalyst sample. A dewar containing liquid nitrogen was raised to surround the glass sample tube and was left in place for approximately 5 min. Next, the stopcock inline with the sample tube and the vacuum manifold was closed and the liquid nitrogen was removed. The sample was allowed to return to room temperature and the stopcock was opened 30 min later. Excess ethylene, which was not adsorbed, was pumped from the sample and the tube was flame sealed under vacuum. After sealing, the samples were either stored in liquid nitrogen or used immediately.

NMR Experiments

All NMR experiments were performed on an Oxford Instruments wide-bore 9.4-T magnet using a home-built console interfaced to a TecMAG unit. At this field strength, the corresponding resonance frequency for ^{13}C and ^{133}Cs are 100.58 and 52.49 MHz, respectively. All carbon chemical shifts are reported with respect to the most shielded resonance of adamantane being 29.50 ppm. Cesium chemical shifts are reported relative to 1.0 M $CsNO_3$. All measurements were made either at room temperature or at 70 K using a Doty Scientific (Columbia, SC) liquid helium probe. This probe was capable of running at 70 K for a period longer than 1 week; thus most long-term experiments were performed on a single sample. Surface samples were packed into a 7-mm zirconia rotor with Kel-F endcaps (Doty Scientific) in an inert N_2 atmosphere glove box (Vacuum Atmospheres).

The solid-state ^{13}C "powder" lineshapes were collected corresponding to mono- and dilabeled ethylene. All room-temperature spectra were collected using cross-polarization with proton decoupling. The optimal contact time was determined to be 250 μs with a 4-s recycle delay. Mono- and dilabeled spectra obtained at 70 K were obtained by using a multiple-contact cross-polarization pulse sequence with proton decoupling (28). In the case of monolabeled ethylene, eight contacts could be achieved with a contact time 250 μs and 60-s recycle delay, whereas dilabeled spectra were obtained using four contacts with all other parameters being held constant. In all cases, the ^{13}C 90° pulse width was 7.0 μs.

We used a Hahn echo to measure the dipolar couplings in $^{13}CH_2\backslash^{13}CH_2$. In this experiment, an echo sequence with cross-polarization is used to create the initial magnetization and proton decoupling was applied during the evolution and refocusing periods. The two rf pulses are separated by a time interval τ and a spin echo is observed at a time τ after the second pulse. In the present case 99.3% of the carbon signal comes from ^{13}C–^{13}C spin pairs; thus, measuring the decay of the echo amplitude as a function of the pulse separation, τ, yields an exponentially damped oscillating signal. From the frequency of the oscillations, the C–C bond distance can be determined directly. Measurements were made by accumulating 1 K transients utilizing a 45-s recycle delay and 7.0 and 13.9 μs for the 90° and 180° pulses, respectively.

The structure of cesium-promoted silver catalysts was further determined by SEDOR spectroscopy. The technique is similar to using the spin echo to measure the C–C bond distance, but in this case the coupling arises between two unlike spins. The experimental constants were 512 transients, 45-s recycle delay, and 2.4- and 4.8-μs cesium selective 90° and 180° pulses. The proton 180° pulse width was 14.0 μs. The fixed time period between cesium pulses was 750 μs. SEDOR experiments were performed on deuterated catalyst surfaces in the presence and absence of ethylene; the SEDOR fraction used in the fitting procedure was the difference between these two measurements.

We also performed combined rotation and multiple pulse spectroscopy (CRAMPS) experiments to determine the extent of the catalyst deuteration using the experimental method previously discussed. Experiments were performed on a Varian Unity+ 300-MHz spectrometer, using a Varian high-power CRAMPS probe. We employed the 24-pulse sequence BR24 (29) with a cycle time of 108 μs, corresponding to a basic pulse spacing of 3 μs. The $\pi/2$ pulse was 1.5 μs with a 5-s recycle delay. MAS speeds were in the range of 2–2.5 kHz in all cases. All shifts are referenced to TMS using tetrahit(trimethylsilyl)silane (TTMSS) as a secondary internal standard.

Data Processing and Calculations

All data processing and calculations were performed using a solid-state analysis package developed within the group (30). The theoretical spectra were generated by calculating an FID of the same length that was acquired experimentally. Furthermore, the calculated FID was zero filled and exponentially multiplied in the same manner as that of the experimental spectrum. Baseline correction on both theoretical and experimental data was performed in the frequency domain by taking the average of the last 10% of the data and repeatedly subtracting this value from the entire spectrum until the difference between iterations was 10^{-6}. Minimization of the residual sum of squares between simulated and experimental data to obtain the NMR parameters was achieved through use of the Levenberg–Marquadt (31) search algorithm obtained from the MINPACK implementation (32). All calculations were performed using either a 4xR4400/150 Silicon Graphics Onyx, a VAX Station 3540, or an IBM RISC 6000/580.

RESULTS AND DISCUSSION

NMR Lineshape Analysis

The system of dilabeled [^{13}C]ethylene supported on a silver catalyst at low temperature constitutes an example of a rigid isolated homonuclear dipolar coupled spin pair. This system is only slightly more complicated by the significant chemical shift anisotropy of the ^{13}C nucleus. In principle, from the static powder lineshape one should be able to obtain the magnitude of the principal components of the chemical shift tensor and the magnitude of the dipolar tensor, i.e., the carbon–carbon bond distance. Since the dipolar tensor is directed along the internuclear vector the mutual orientation of the two tensor interactions can be resolved with respect to the molecular frame. This information may be obtained by nonlinear least-squares analysis of the experimental powder pattern using a function that depends on the following six parameters: δ_0, the isotropic chemical shift; $\Delta\delta_{cs}$, the chemical shift anisotropy; η, the asymmetry parameter; r_{cc}, the carbon–carbon bond distance; and the two Euler angles α and β, which relate the principal axis system of the chemical shift tensor with respect to the dipolar tensor.

Due to signal-to-noise considerations we have followed a strategy outlined by Koons *et al.* (30) where the number of parameters in the fit is reduced by performing separate experiments on monolabeled [^{13}C]ethylene to determine the chemical shift parameters separately. In this paper we further reduced the number of parameters used to fit the dilabeled data by performing a "slow-beat" Hahn echo experiment (33) to isolate the dipolar coupling. In this experiment the chemical shift is removed by refocusing the interaction by using a π pulse. The amplitude of the resulting stimulated echo is, to first order, modulated solely by the dipolar interaction. The dipolar coupling constant is obtained by fitting the amplitude of the echo as a function of echo pulse separation while allowing for T_2 relaxation.

The monolabeled [^{13}C]ethylene spectra are shown in Fig. 1 together with the simulated spectra obtained by nonlinear least-squares analysis. The three experimental spectra represent cesium loadings of 0, 14, and 26% by weight relative to silver. The principal components derived from the fits are given in Table 1 together with values for ethylene diluted in an argon matrix (23). Again we observe the characteristic movement of the isotropic shift to increased shielding, indicative of the silver interacting with the ethylene in a π-bonding fashion. On addition of the cesium promoter the isotropic shift decreases further by 7 ppm for the 26% Cs case. When the tensor elements are analyzed,

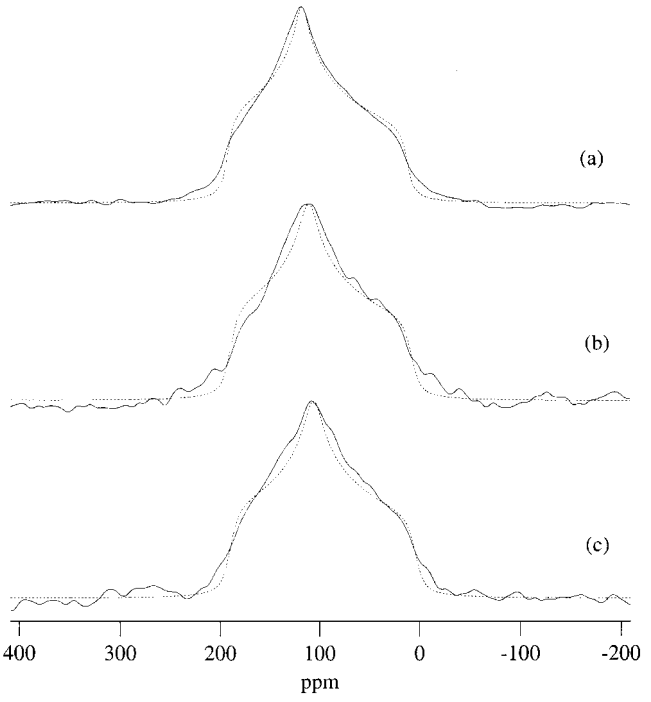

FIG. 1. Overlap of the experimental and simulated lineshapes of monolabeled [^{13}C]ethylene corresponding to (a) 0%, (b) 14%, and (c) 25% (wt) cesium.

the largest changes on the addition of cesium are observed in the δ_{22} and δ_{33} elements where they steadily decrease. This would indicate that the cesium affects the ethylene in a different manner than the action of the silver where the δ_{11} element was most affected. We shall see later that this difference is significant in terms of discriminating different equilibrium models and in the light of the SEDOR results to be discussed later.

In previous studies Wang and Ellis (24) explained the changes observed in static dipolar coupled ethylene spectra as a function of cesium loading to an increase in the carbon–carbon bond distance. This analysis kept the relative orientation of the chemical shift and dipolar tensors constant. In this study we have measured the internuclear carbon distance separately. This experiment used a Hahn echo sequence, $\pi/2$–τ–π–τ–acquire, where τ is a variable time delay that is incremented in a series of separate experiments. The dephasing of the net magnetization after the $\pi/2$ pulse due to the chemical shift interaction during period τ is refocused by the π pulse after the second τ period. Dephasing due to the homonuclear interaction is unaffected by the refocusing pulse, causing the spins to accumulate a phase error. This phase error follows a $\pm k_1(3\cos^2\theta - 1)$, with $k_1 = (3/2)\gamma^2\, h/2\pi\mu_0/(4\pi)(r_{cc})^{-3}$ as a function of τ, which leads to a modulation in the echo amplitude as

$$G(\tau) = \cos(k_1(3\cos^2\theta - 1)\tau), \qquad [1]$$

where θ ranges over all possible orientations. This result indicates that the echo amplitude oscillates with τ at a frequency dictated by the dipolar coupling k_1. This was first noted by Hahn, who called it a "slow beat" (33).

Slichter and Wang used this technique to study acetylene and ethylene adsorbed on supported platinum catalysts (34–36). They showed that the analysis of the slow-beat oscillations requires a knowledge of the dynamics and chemical shift tensors of the two homonuclear coupled spins. By working at 77 K, the ethylene is assumed to be static. In all previous work with ethylene adsorbed to silver, only a single chemical shift principal axis system was required to describe the shielding for both carbon nuclei. Thus, we have assumed in this study that the two carbons share the same chemical environment and have similar resonance frequencies for all catalyst systems studied. A discussion of the consequences of having dissimilar principal axis systems relating to the results to be outlined is given in the Appendix.

In the analysis of the slow-beat oscillations, we have calculated the echo amplitude $G(\tau)$ as a function of τ according to the equation

$$G(\tau) = \exp\left[\frac{-2\tau}{T_2}\right]\int_0^{2\pi}\cos(k(3\cos^2\theta - 1)\tau)\, d\theta, \qquad [2]$$

where T_2 is the relaxation time and $k = k_1$, assuming both carbons share the same chemical shift and principal axis system, e.g., the carbons are "like" nuclei, and $k = k_u = \gamma^2 h/2\pi\mu_0/(4\pi)(r_{cc})^{-3}$ if the carbon nuclei are "unlike" in terms of the magnitude or orientation of their CSAs. A function comprising Eq. [2] was written and approximated by standard numerical integration.

We first analyzed the spin-echo measurements corresponding to dilabeled ethylene adsorbed on a nonpromoted silver surface for both like and unlike chemical shift principal axis systems. For the unlike model, r_{CC} was determined to be less than an Ångstrom, whereas by fitting the data assuming a single principal axis system for both carbon nuclei, we obtained $r_{CC} = 1.342 \pm 0.009$ Å, a value much closer to the gas-phase bond distance for ethylene of 1.340 Å (37) (value extracted for T_2 was 200 ± 6 ms). From the results

TABLE 1

Chemical Shift Parameters Obtained from Least-Squares Analysis of the Lineshapes Corresponding to Monolabeled Ethylene Adsorbed on Promoted and Nonpromoted Silver Catalysts

	Ref. (18)	0% Cs		14% Cs		26% Cs	
	value	Value	Error	Value	Error	Value	Error
δ_0 (ppm)	132	107.0	0.2	100.5	0.3	99.4	0.2
δ_{11} (ppm)	239	191.5	0.3	188.2	0.4	189.3	0.3
δ_{22} (ppm)	129	117.7	1.5	107.5	1.9	105.4	1.5
δ_{33} (ppm)	29	11.8	0.3	5.8	0.4	3.5	0.3
$\Delta\sigma$ (ppm)	−155	−142.8	0.8	−142.1	0.9	−143.9	0.8
η	1	0.78	0.05	0.85	0.05	0.87	0.05

TABLE 2

Summary of the Dilabeled Ethylene Lineshape Analysis[a]

Best fit to Part A					Best fit to Part B			
% Cs	r_{CC} (Å)	Error	T_2 (ms)	Error	α°	Error	β°	Error
0	1.342	0.009	204	5	99	3	96	1
14	1.355	0.008	203	6	104	3	94	1
26	1.368	0.009	203	5	110	3	95	1

[a] Part A was obtained by analyzing the slow beat of the spin echo, whereas Part B was determined from the least-squares fitting of the static dilabeled ethylene lineshapes by the method described in the text.

of this fit, we concluded that the two carbons shared the same principal axis system and all subsequent analyses of the slow-beat experiments on the promoted catalyst systems were performed in this manner. Table 2A summarizes the spin-echo measurements made on 10 wt% silver catalysts promoted with 0, 14, and 26% by weight Cs/Ag. The results indicate a systematic change in the bond distance as a function of added promoter, namely a change of 0.026 Å going from the nonpromoted catalyst to one that contains 26 wt% cesium. Figure 2 summarizes the integrated intensity versus the τ values used in the spin echo and the best fit to the data.

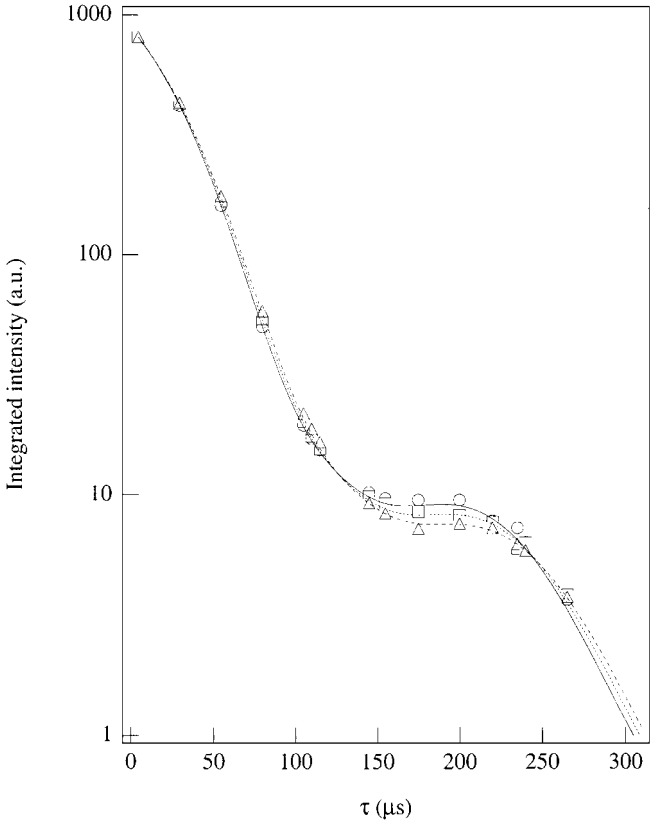

FIG. 2. Slow-beat data obtained from dilabeled ethylene on promoted silver catalysts with (circle) 0% (square) 14%, and (triangle) 26% cesium along with the respective best fits to the data at 1.342, 1.355, and 1.368 Å.

Based on this independent determination of the bond distance from the spin-echo experiment and the chemical shift information from the analysis of the monolabeled data the relative orientations of the two tensor interactions with respect to the molecular frame could be derived from dilabeled ethylene lineshapes via nonlinear least-squares analysis. In all three cases, the uncertainty predicted by the MINPACK routine COVARD for the β angle was smaller than the uncertainty predicted for the α angle. However, there appeared to be two minima with almost the same residual sum-of-squares value associated with the β angle. This gave rise to a family of solutions with values centered around $95^\circ \pm 1^\circ$ and $85^\circ \pm 1^\circ$ depending on the choice of the initial estimate, with the former being marginally more preferred in all three lineshapes that were analyzed. Thus, we accepted the value for β obtained for the solution near $95^\circ \pm 1^\circ$. However, there was no trend in this angle beyond experimental error, which indicated it did not change substantially in the presence or absence of cesium. On the other hand, the α angle changed in a systematic fashion from 96° to $110^\circ \pm 3^\circ$ as a function of added cesium, indicating that the orientation of the δ_{22} element deviated from the carbon–carbon internuclear vector with increasing loading. This result indicated that the effect of the cesium was to increase the strength of the ethylene–silver interaction to the point where symmetry constraints of the ethylene molecule were no longer applicable. This loss of symmetry does not affect the analysis of the "slow-beat" experiments (see Appendix). The final results from the dilabeled fits are given in Fig. 3, which shows the comparison of experimental lineshapes and simulated spectra using this fitting strategy; the parameters extracted are given in Table 2B.

SEDOR Determination of Cesium–Ethylene Distance

To determine the nature of the ethylene–cesium interaction, i.e., whether the cesium was close to or far away from the ethylene, the ^{1}H–^{133}Cs heteronuclear dipolar interaction between the surface cesium and the ethylene protons using a fully deuterated catalyst was investigated. We used the SEDOR experiment to measure ^{1}H–^{133}Cs dipolar couplings. In this experiment, the π pulse of the Hahn spin echo is replaced by two π pulses, one for ^{1}H and the other for ^{133}Cs. In the original SEDOR pulse sequence given by Emshwiller *et al.* (26), (^{133}Cs)–$\pi/2$–τ–π–τ–acquire and (^{1}H)–τ–π–, the simultaneous π pulses on the cesium and proton channel effectively cause, after the second evolution period τ, the chemical shift to be refocused and the heteronuclear dipolar coupling to remain (26). In this way, the cesium spins continue to dephase during the second τ interval due to any heteronuclear dipolar coupling present and a reduction in the echo amplitude is observed relative to the measurement without the proton π pulse. From the

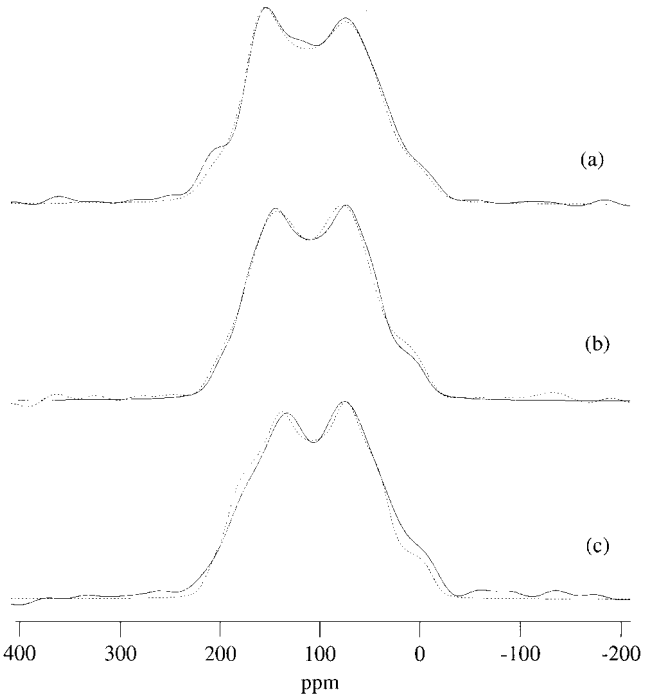

FIG. 3. Overlap of the experimental (solid line) and simulated (dashed line) static lineshapes of dilabeled [^{13}C]ethylene on supported silver γ-alumina catalyst for (a) 0%, (b) 14%, and (c) 26% cesium (wt).

difference of these two measurements, the interaction between the two neighboring nuclei can be determined.

We used the SEDOR experiment discussed by Slichter and Wang (34–36) where the time between the cesium $\pi/2$ and π degree pulses is constant and the ^{1}H pulses are applied at different times relative to the first ^{133}Cs pulse, e.g., (^{133}Cs)–$\pi/2$–τ_f–π–τ_f–acquire and (^{1}H)–τ_v–π–. In Slichter's modified SEDOR experiment, the echo amplitude is measured as a function of τ_v, i.e., the separation between the first cesium $\pi/2$ degree pulse and the proton π degree pulse. Because τ_f is kept constant, only one spin-echo measurement in the absence of the π-degree proton pulse is required to observe the difference in echo amplitude; this difference is called the SEDOR signal. The SEDOR fraction (SF) is given by

$$\mathrm{SF} = \frac{S - S'}{S} = 1 - \frac{S'}{S}, \qquad [3]$$

where S is the spin-echo amplitude in the absence of the proton pulse whereas S' is the echo amplitude when the proton π pulse is applied. According to these definitions, cesium nuclei not coupled to protons will not be affected by the additional proton pulse during the evolution period and no change in the echo amplitude will be observed and hence the SEDOR fraction will be zero.

From the analysis of both the slow-beat data and the chemical shift tensors of monolabeled ethylene, we have determined that the results are consistent with ethylene weakly interacting with silver through its π electrons: e.g., the ethylene remains intact in the presence of silver and promoted silver catalysts at or below room temperature. Thus, to model the SEDOR fraction we obtained experimentally, we must consider that the protons originate from one or more molecules of ethylene. We have considered the following ways in which cesium may interact with one or more molecules of ethylene:

1. Cs along the twofold axis perpendicular to the plane of ethylene
2. Cs in the plane and along the side of ethylene
3. Cs in the plane and nearest the end of ethylene
4. Two ethylene molecules in the configuration given by Model 2
5. Two ethylene molecules in the arrangement of Model 3

Figure 4a illustrates schematically the models we have used to describe the cesium–ethylene interaction.

To compute the SEDOR fraction, in Models 1–3, a total of four cesium–proton internuclear vectors must be considered, whereas Models 4 and 5 require the treatment of eight vectors. To simplify the "Wignerology" required to resolve the relationship between the internuclear vectors and the external magnetic field, we defined a coordinate system fixed with respect to the mutual orientation of cesium and the ethylene molecule for each model. In this way, each of the protons can be given an (x, y, z) coordinate and the normalized vector connecting a given cesium and proton can then be constructed. By incrementing the magnetic field vector through all orientations θ and ϕ, all possible internuclear vector projections can be determined. Figure 4b shows a representative coordinate system defined for each model and Table 3 summarizes the coordinates used to

TABLE 3

Summary of the Coordinates Used to Locate the Protons in the SEDOR Models Given in the Text

1	1	$r_{CH}\sin\gamma$	$a+c$	$b\tan\beta$	$a = 0.5\, r_{CC}$
	2	$r_{CH}\sin\gamma$	$a+c$	$b\tan\beta$	$b = (a^2 + (r_{CH})^2)^{1/2} - (2ar_{CH}\cos\alpha)^{1/2}$
	3	$r_{CH}\sin\gamma$	$-(a+c)$	$b\tan\beta$	$c = r_{CH}\tan\gamma$
	4	$r_{CH}\sin\gamma$	$-(a+c)$	$b\tan\beta$	$d = r_{CH}\sin\gamma$
					$\alpha = (180 - 0.5\theta_{HCH})$
					$\beta = \sin^{-1} b/r_{01}$
					$\gamma = 90 - 0.5\theta_{HCH}$
2	1	0	$a+b$	d	$a = r_{CH}\sin(90 - 0.5\theta_{HCH})$
	2	0	$a+b$	$2c+d$	$b = 0.5 r_{CC}$
	3	0	$-(a+b)$	$2c+d$	$c = r_{CH}\cos(90 - 0.5\theta_{HCH})$
	4	0	$-(a+b)$	d	$d = r_{01}\cos\beta$
					$\alpha = (180 - 0.5\theta_{HCH})$
					$\beta = \sin^{-1}((a+b)/r_{01})$
3	1	0	a	c	$a = r_{CH}\sin(90 - 0.5\theta_{HCH})$
	2	0	a	$r_{CC}+2b+c$	$b = r_{CH}\cos(90 - 0.5\theta_{HCH})$
	3	0	$-a$	$r_{CC}+2b+c$	$c = ((r_{01})^2 - a^2)^{1/2}$
	4	0	$-a$	c	

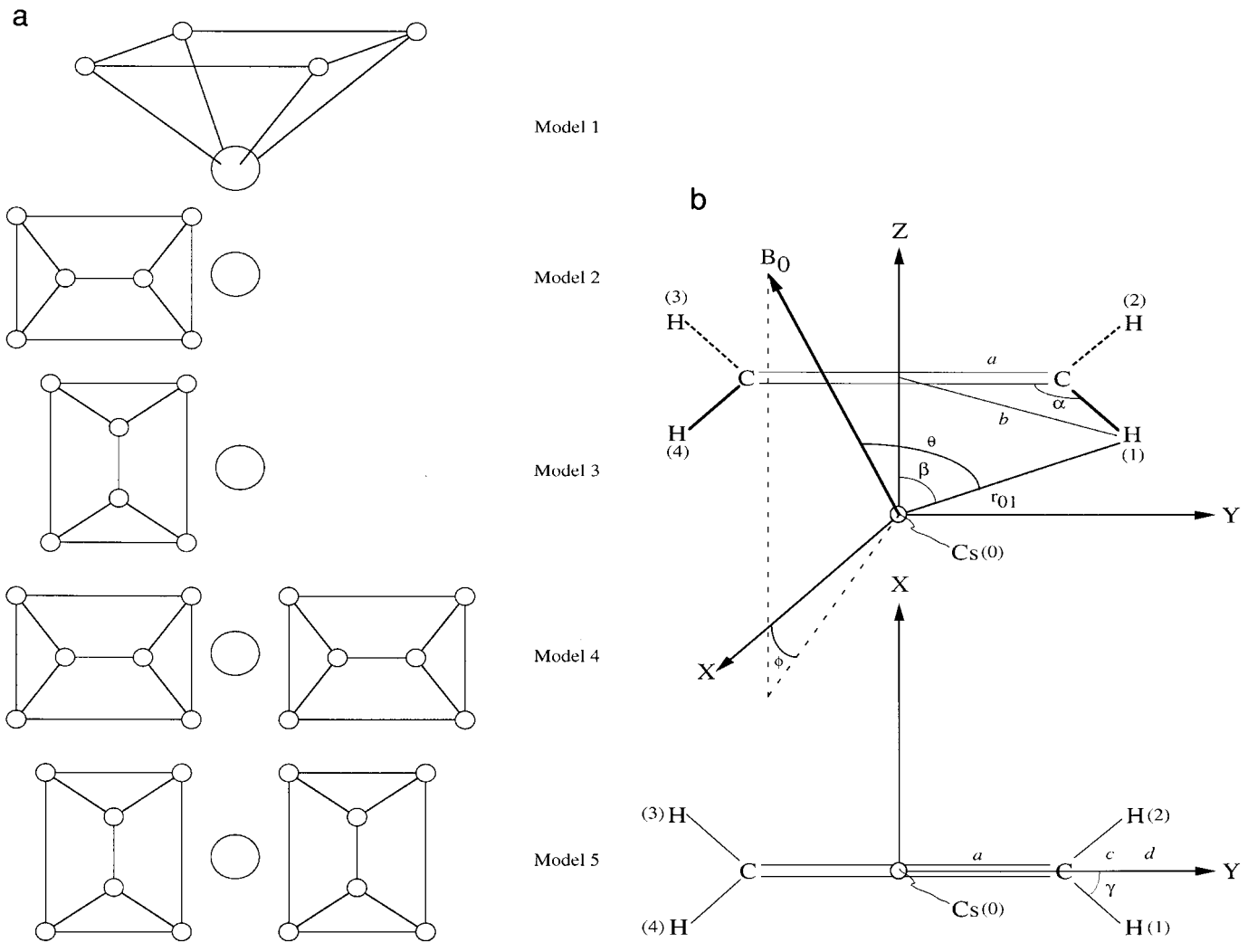

FIG. 4. (a) Summary of the various models employed to fit the proton–cesium SEDOR fraction. The small open circles denote either protons or carbon atoms and the larger circles denote cesium atoms. (b) SEDOR model 3 with cesium along the twofold axis perpendicular to the plane of the ethylene molecule.

locate the protons. Using this scheme, the evaluation of the SEDOR fraction reduces to

$$\mathrm{SF} = \int_0^{2\pi}\int_0^{2\pi} (1 - \cos(k_u \tau_v)) \sin\theta \, d\theta \, d\phi, \qquad [4]$$

with

$$k'_u = \gamma_1\gamma_2\hbar \sum_{i=1}^{n} r_{0,i}^{-3}(3\cos^2\theta - 1), \qquad [5]$$

where $\cos\theta = B_0 R_i$ with $B_0 = (\sin\theta\cos\phi, \sin\theta\sin\phi, \cos\theta)$ and R_i is given by the vector containing the normalized (x, y, z) coordinates of the protons in ethylene for each of the respective models given in Table 3. The integral in Eq. [4] is approximated using Conroy–Wolfsberg (38) integration and the SEDOR fraction is subsequently scaled by the number of points sampled on the sphere. Each modeling function was incorporated into a MINPACK nonlinear least-squares optimization routine. One independent cesium– proton bond distance was optimized by the MINPACK routine in all five models.

The catalyst used for the SEDOR measurements was 14 wt% cesium which was deuterated as described. We characterized the extent of proton exchange as a function of time by diffuse reflectance FTIR. The results shown in Fig. 5 clearly indicate the exchange of labile protons for deuterium. In addition, we have further characterized the support by proton CRAMPS experiments. Figure 6 shows the CRAMPS spectrum obtained for (a) the starting catalyst material, (b) after the vacuum heating step at 270°C described, and (c) after the deuterium exchange and vacuum, heating step (Fig. 6c corresponds to the IR spectrum

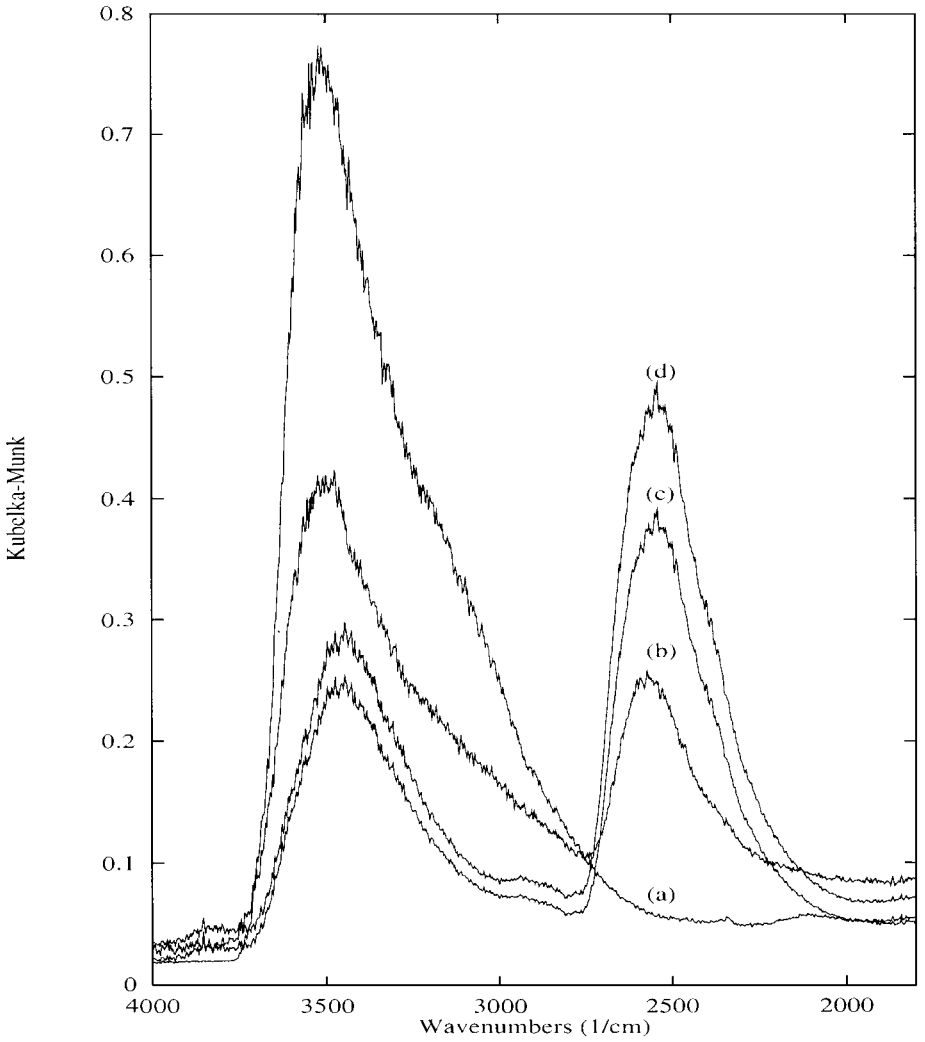

FIG. 5. Diffuse reflectance FTIR spectra obtained from 1.0 mg silver catalyst diluted in 1.0 mg KBr as a function of deuteration time. The reaction time was (a) 0, (b) 1, (c) 4, and (d) 8 h.

obtained under the same conditions given in Fig. 5d). Furthermore, the SEDOR experiment was repeated in the presence and absence of monolabeled ethylene and the subtraction of the two measurements was used to determine the SEDOR signal. Measurements of the spin-echo amplitude in the absence of the proton π pulse for $\tau_f = 750$ μs were also performed in the presence and absence of ethylene; there was effectively no difference in the values obtained.

We analyzed the SEDOR fraction first with the model proposed by Carter and Goddard, Model 1 (22). The best fit to the data with this model produced a SEDOR fraction of 0.6 for the longest values of τ_v. We then manually incremented the bond distance from 1.0 to 10.0 Å in steps of 0.5 Å and found no value for r_{HCs} that gave a SEDOR fraction that approached 0.8 and matched the shape of the curve seen experimentally. Furthermore, we were not able to obtain a satisfactory fit to the SEDOR data with any of the models that used one ethylene and one cesium center (Models 1–3). However, when considering Models 4 and 5, each assuming that two ethylene molecules are associated with a single cesium center, we were able to fit the experimental result (indicating that the protons from ethylene can be considered to be close to cesium, specifically with four close and four are further away). Model 4 produced the best fit in terms of the residual sum of squares; however, Model 5 could not be eliminated as a possibility because of the large uncertainty in the measurements. Figure 7 shows the results of the SEDOR experiment compared with predictions from the various models. The best fits to the indicated models were for Model 1 with $r_{01} = 4.38$ Å, Model 4 with $r_{01} = 4.40$ Å ($r_{02} = 6.25$ Å implicitly), and Model 5 with $r_{01} = 4.52$ Å ($r_{02} = 7.78$ Å).

The results of the SEDOR experiment clearly suggest the cesium is associated with the ethylene protons (implying that the cesium is on the surface of the silver). However, this measurement does not imply that cesium is associated

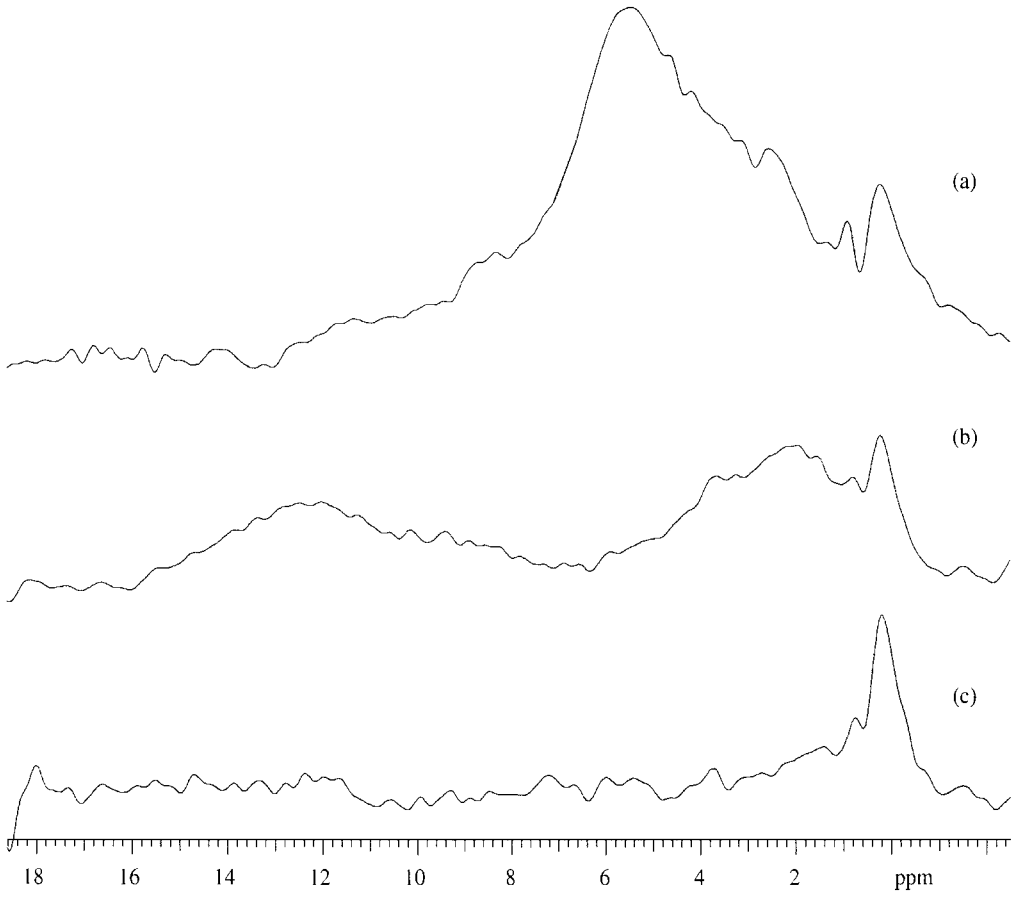

FIG. 6. Proton CRAMPS NMR spectra of silver catalyst samples that were treated as follows: (a) 370°C calcination in air, (b) same as in (a) with an additional 4-h heating step at 270°C and 10^{-5} Torr, and (c) same as in (b) after 8-h deuteration reaction. All spectra are plotted on the same vertical scale.

only with the silver surface. There is a substantial excess of cesium present and, surely, the cesium is associated with the support as well. The SEDOR experiment provides a selective means to visualize the cesium associated with the silver surface.

To further understand the nature of the cesium–anion interaction we performed ^{133}Cs NMR experiments on CsCl on an alumina support in the presence and absence of silver. As one might expect from elementary chemistry considerations, the NMR data indicated that the chloride anion was not associated with the cesium in the presence of silver. The chemical shift (data not shown) was consistent with an oxygen anion, presumably as a result of picking up carbonate from the atmosphere. The resulting ^{35}Cl NMR signal is consistent with the presence of AgCl on the surface. Although from these examples it is difficult to ascertain the exact nature of the interaction between the chloride anion and the silver, they clearly suggest that neither the anion nor the cation of the cesium salt participates in a chemical process that leads to an association with surface sites of γ-alumina.

From all of the NMR measurements, it is clear that the cesium has a profound effect on the ethylene molecule. However, from these results alone the chemical state of the cesium is not clear. SEDOR and SEM-XF measurements have indicated that the cesium is associated with the silver and is present in the form of a salt. We do not know the structural details associated with the salt, i.e., whether it is solvated, etc., but we do know that the anion must be proximal to the cesium to preserve charge balance. Thus, because of the size of the cation–anion pair relative to the size of a silver atom, it is unlikely that the cesium salt will be distributed throughout the silver metal. Rather, it will be preferentially found on the surface. Analysis of both the monolabeled lineshapes and the SEDOR data support this argument as they indicate that cesium is "near" the actual site where ethylene adsorbs onto the silver surface. Specifically, analysis of the SEDOR fraction indicates that the ethylene protons were approximately 4.5 Å from the cesium and the monolabeled data indicate that the cesium salt is close enough to the ethylene to induce a change in the electron density (or, more properly, the current density) around the carbon atoms. It is important to remember that the structural results were obtained at low temperatures and in the absence of reactant oxygen. Hence, the

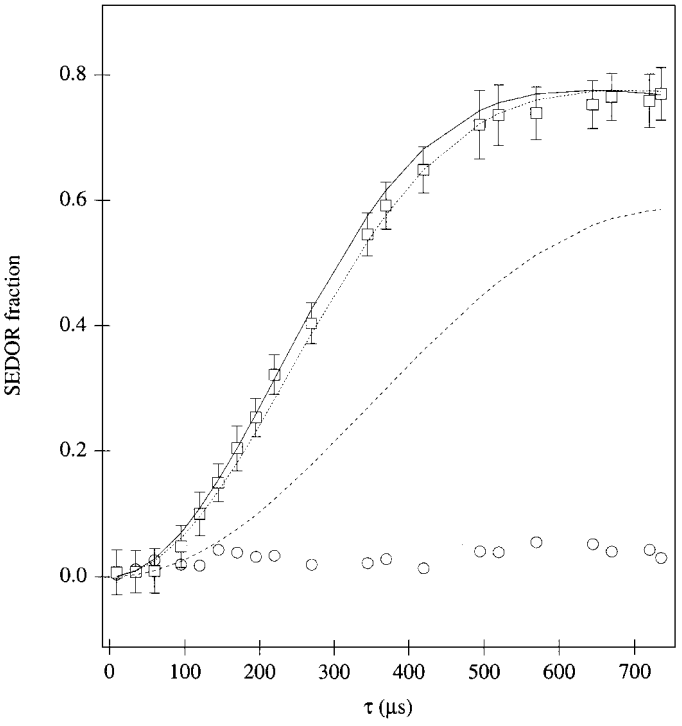

FIG. 7. SEDOR fraction in the presence (square) and absence (circle) compared with predictions from models: Model 1 (dashed line), Model 4 (solid line), Model 5 (dotted line).

structural data represent a framework for discussion of catalytic events, but do not reflect the dynamics nor potential structural changes that may arise due to the increased temperature associated with real catalysis.

The problem that remains to be solved, however, is how the cesium affects the ethylene. It is well known that the magnitude of the anisotropic chemical shift depends on the current density perpendicular to the directions specified by the three principal axes of the interaction (39). Thus when the orientation of the CSA in the molecular frame is well characterized, then this information is indicative of the electronic characteristics of the molecule. As was mentioned before, Zilm and Grant (23) showed that the orientation of the chemical shift tensor in the molecular frame of ethylene follows the principal elements parallel to the three C_2 rotation axes of the molecule. From this work, δ_{33} was found to be normal to the molecular plane, δ_{22} to lie along the C–C bond, and δ_{11} to lie in the molecular plane, but perpendicular to the C–C bond. Thus, the tensor information can be shown to indicate the following characteristics for the ethylene molecule:

1. δ_{11} component: depends on the carbon–carbon π and σ electrons.

2. δ_{22} component: involved in double-bond mixing of the π electrons with the carbon's σ electrons external to the double bond.

3. δ_{33} component: involves electrons from sp^2 hybrid orbitals appearing in the σ component of the double bond and in the external σ bonds.

From this set of rules, we can interpret the changes in the CSA of ethylene in terms of electron density in the molecular frame. First, consider CSA changes observed when going from ethylene in an argon matrix to ethylene adsorbed to a nonpromoted silver catalyst. Although all elements of the chemical shift tensor changed to a certain degree, the change in the δ_{11} element was the most significant. This can be understood because the δ_{11} element is affected principally by the carbon π electrons. In addition, this is consistent with the proposed π-bond interaction expected classically and with the previous results given by Chin and Ellis (20). Next, consider the monolabeled ethylene lineshapes observed in the presence of 14 and 26 wt% cesium. It can be seen from Table 1 that there is a 7-ppm change in the isotropic chemical shift comparing the nonpromoted catalyst with one that contains 26 wt% silver. Furthermore, the largest change in the chemical shift tensor (measured relative to the 0 and 26% samples) occurred in the δ_{22} and δ_{33} elements. This would suggest that, on "average," the cesium interacts in the plane of the ethylene molecule. Use of the word "average" here does not imply a dynamic process; rather, it is meant to point out that we do not know any details of how much the Cs^+ deviates from the plane of the ethylene molecules. We only considered simple models that could illustrate how the cesium could potentially interact with the surface adsorbed ethylene. These observations, however, are inconsistent with the proposed mechanism where cesium sits on top of the oxygens present in the 4-coordinate trough as proposed by Carter and Goddard (22).

From the monolabeled, SEM-XF, and SEDOR measurements, we have determined that the state of the cesium is consistent with it being present on the surface of the silver in the form of a salt, a cation–anion pair. However, the question remains as to how the cesium induces an increase in the C–C bond length in the ethylene molecule. As we have previously mentioned, ultrahigh vacuum investigations involving transition and alkali metals indicated a change in the binding affinity and reactivity of coadsorbed gases due to the lowering of the workfunction of the metal substrate. Because we have also observed this property in the current system, exemplified by the measured increase in the carbon–carbon bond distance, we propose that this is also occurring with the cesium present as a salt.

In the promoted surfaces, we propose that the presence of a polarizable cation–anion pair reduces the electrostatic potential near the adsorption site and the "local" workfunction of the surface is lowered. The reduction in the workfunction facilitates electron backdonation from the Fermi level of the silver to antibonding π^* orbitals of the ethylene and the carbon–carbon bond distance increases. The

view described here is exactly what would be expected if the experiments were performed under ultrahigh vacuum conditions and if the cesium atoms were sputtered onto a silver surface. It is, however, clear that these conditions do not correspond to the conditions under which the NMR experiments were performed, with the most obvious difference being between cesium atoms and cesium ions. However, we believe the same rationale applies where the cesium atom can be replaced by a polarizable ion pair. In this model, the polarizability of the cation–anion pair determines how well (or how poorly) a given cesium salt can mitigate the surface dipole and lead to the observed promoter effects. Likewise with the Lang model, for this scheme to explain the observed results, the cesium salt must make direct contact with the silver surface and not go through an intervening oxide anion as previously suspected.

If this assertion that a polarizable cation–anion pair can assume the role of the cesium metal in the description of the reduction of the workfunction, our current observations should represent the first connection between the UHV catalytic results and solid-state NMR. Furthermore, this connection, when combined with the SEDOR distance information, demonstrates a novel measure of the reduction in the surface dipole. In the current case, the surface dipole is reduced over several silver atoms in the vicinity of the cesium salt.

CONCLUSIONS

The effects of cesium promoters on silver catalysts, supported on γ-alumina, were studied by adsorbing either $^{13}CH_2CH_2$ or $^{13}C_2H_2$ $^{13}CH_2$ onto the surface and performing low-temperature (70 K) solid-state ^{13}C NMR measurements on the ethylene. Selective isotopic enrichment was used to investigate the electronic environment present in and around the ethylene molecule as a function of promoter concentration. Changes in the spectroscopic parameters describing the ethylene lineshapes were then used to determine the structure of the ethylene molecule on the surface and to probe the changes induced by the added cesium promoters.

The complete chemical shift tensor of ethylene was deduced through a nonlinear least-squares analysis of the monolabeled ethylene lineshapes; the results indicate that the ethylene binds to the silver surface through a weak π-bond interaction which increases in strength as a function of cesium loading. Furthermore, these results indicated that both the δ_{22} and the δ_{33} elements of the chemical shift tensor change as a function of cesium loading, implying that the cesium interacts with the ethylene in the plane of the molecule. The changes in the tensor elements have been attributed to steric effects between the C–H σ bonds and the cesium salts.

The carbon–carbon bond distance, r_{CC}, was measured directly using the Hahn echo sequence which eliminated the chemical shift tensor. From these measurements, it was found that the bonding between the silver and the ethylene is symmetric with respect to each carbon atom and that the ethylene carbon–carbon bond distance increased as a function of increasing concentration of cesium promoter. The increase observed in r_{CC} has been ascribed to a reduction in the workfunction of the silver around the adsorbed alkali—this is thought to facilitate electron backdonation from the Fermi level of the silver to antibonding π^* orbitals. Furthermore, the independent determination of the carbon–carbon bond distance from the spin-echo experiment was fixed in the least-squares analysis of the dilabeled ethylene lineshapes to determine the Euler angles. The result of this fitting indicated that the orientation of the δ_{22} element of the chemical shift tensor was rotating away from the r_{CC} internuclear vector with increasing cesium loading, demonstrating that the effect of the cesium was to increase the strength of the ethylene–silver interaction to the point where symmetry constraints of the ethylene molecule were potentially no longer applicable. By this we mean that the surface interaction in combination with the added promotor and the lack of motion could potentially make the carbons nonequivalent.

In an effort to understand the state of the cesium in the catalyst system, a SEDOR experiment was devised to measure the distance between the ethylene protons and the cesium centers. The results, from modeling the experimental observations, demonstrate that two ethylene molecules were associated with a single cesium.

Finally, we proposed that the experimental trends observed in the present study were similar to the experimental results obtained from the ultrahigh vacuum surface techniques, and we suggested that these assertions represent the first connection between the UHV catalytic results and solid-state NMR.

APPENDIX

Because the inversion symmetry of the ethylene molecule is lost at higher promoter concentrations, we generalized our simulation to consider this possibility. As outlined in Ref. (30), our original simulation was derived by expressing the dipolar interaction in the PAS frame of the chemical shift tensor and then relating this frame to the laboratory axis system. In the current case, the PAS frames of the two chemical shift tensors are allowed to be distinguishable. We begin by relating the individual chemical shift tensor axis systems to the PAS frame of the dipolar tensor and subsequently rotating the dipolar axis system into the LAB frame of reference. The complete Hamiltonian is given as $H = H^{CS}(A) + H^{CS}(B) + H^{DI}$, where A and B label the individual nuclei. Further, H^{CS} and H^{DI} denote the chemical

shift and dipolar Hamiltonians, respectively, in their respective PAS frames. The relevant Wignerology follows:

$$H = c^{CS}T^{CS}_{0,0}\left(\rho^{CS}_{0,0}(A) + \rho^{CS}_{0,0}(B)\right) + c^{CS}\sum_{i=A,B}\sum_{n}T^{CS}_{2,n}\sum_{m}\mathcal{D}^2_{m,0}(-\phi,-\theta,0)\cdot\mathcal{D}^2_{m,n}(-\gamma(i), -\beta(i),-\alpha(i))\rho^{CS}_{2,m}(i) + c^{DI}T^{DI}_{2,0}\sum_{n}\mathcal{D}^2_{n,0}(-\phi,-\theta,0)\rho^{DI}_{2,n} \quad [A1]$$

with constants $c^{CS} = \gamma$ and $c^{DI} = -2\gamma^2(h/2\pi)$ $[\mu_0/4\pi]$. The spin terms are defined as

$$T^{CS}_{2,0} = I_Z B_Z, \quad T^{CS}_{2,0} = \sqrt{\frac{2}{3}} I_Z B_Z, \quad T^{CS}_{2,\pm 2} = 0, \qquad T^{DI}_{2,0} = \frac{1}{\sqrt{6}}(2I_{Z1}I_{Z2} - \frac{1}{2}(I_1^+ I_2^- + I_1^- I_2^+)), \quad [A2]$$

and the spatial tensors have the following definitions:

$$\rho_{0,0} = \delta^{CS}_0, \quad \rho^{CS}_{2,0} = \sqrt{\frac{2}{3}}\delta_{CS}, \quad \rho^{CS}_{2,\pm 1} = 0, \qquad \rho^{CS}_{2,\pm 2} = -\frac{1}{2}\delta_{CS}, \quad \rho^{DI}_{2,0} = \sqrt{\frac{3}{2}} r_{12}^{-3} \quad [A3]$$

We implemented this methodology and performed simulations with the parameters in Tables 1 and 2 for 0, 14, and 26% cesium samples. For the 26% cesium sample, the two sets of Euler angles used were $\alpha_1 = 110^\circ$, $\beta_1 = 95^\circ$, $\gamma_1 = 0$, $\alpha_2 = -\alpha_1$, $\beta_2 = -\beta_1$, and $\gamma_2 = 0$. We determined from the results of all three simulations that there is essentially no difference (after the powder average) between the spectra calculated by this manner or and those calculated by the method given in Ref. (30). Furthermore, we found from similar calculations that the maximum separation of individual crystallites was less than 500 Hz by allowing the chemical shift reference frames to be noncongruent. Thus we used the original simulation function for all nonlinear least-squares optimizations.

ACKNOWLEDGMENTS

The authors acknowledge support from Pacific Northwest National Laboratory, which is a multiprogram national laboratory operated by Battelle Memorial Institute for the U.S. Department of Energy under Contract DE-AC06-76RLO 1830. The initial phase of this research was carried out while P. D. Ellis and J. Wang were at the University of South Carolina. J. Wang acknowledges partial support from Union Carbide Corporation, Charleston, West Virginia. Likewise during this period, P. D. Ellis was partially supported by NSF Grant CHE89-21632.

REFERENCES

1. Law, G. H., and Chitwood, H. C., U.S. Patent 2,279,469.
2. Lefort, T. E., French Patent 729,952.
3. Thomas, C. L., "Catalytic Processes and Proven Catalysts." Academic Press, New York, 1970.
4. Barteau, M. A., and Madix, R. J., *Surf. Sci.* **97**, 101 (1980).
5. Metcalf, P. L., and Harriott, P., *Ind. Eng. Chem. Process Des. Dev.* **11**, 478 (1972).
6. Kagawa, S., Iwamoto, M., and Morl, H. J., *J. Phys. Chem.* **85**, 434 (1981).
7. Van Santen, R. A., and Knipens, H. P. C. E., *Adv. Catal.* **35**, 265 (1987).
8. Dean, M., and Bowker, M., *J. Catal.* **115**, 138 (1989).
9. Jorgensen, K. A., and Hoffman, R. J., *J. Phys. Chem.* **94**, 3046 (1990).
10. Pacchioni, G., and Bagus, P. S., *Phys. Rev. B* **40**, 6003 (1989).
11. Engelhart, H. A., and Menzel, D., *Surf. Sci.* **57**, 591 (1976).
12. Rovida, G., *J. Phys. Chem.* **80**, 1150 (1976).
13. Rovida, G., and Pratesi, F., *Surf. Sci.* **52**, 452 (1975).
14. Barteau, M. A., and Madix, R. J., *Surf. Sci.* **97**, 101 (1980).
15. Muscat, J. P., and Batra, I. P., *Phys. Rev. B* **34**, 2889 (1986).
16. Bonzel, H. P., *Surf. Sci. Rep.* **8**, 43 (1987).
17. Lang, N. D., *in* "Solid State Physics" (H. Ehenreich, F. Seitz, and D. Turnball, Eds.), Vol. 10, p. 1011. Academic Press, New York, 1973.
18. Campbell, C. T., *J. Catal.* **99**, 28 (1986).
19. Wang, J., and Ellis, P. D., *J. Am. Chem. Soc.* **115**, 212 (1993).
20. Chin, Y., and Ellis, P. D., *J. Am. Chem. Soc.* **115**, 204 (1993).
21. Aris, K. R., and Brown, J. M., *J. Organomet.* **42**, C67 (1972).
22. Carter, E. A., and Goddard, W. A., III, *Surf. Sci.* **209**, 289 (1989).
23. Zilm, K. W., and Grant, D. M., *J. Am. Chem. Soc.* **103**, 2913 (1980).
24. Wang, J., and Ellis, P. D., *J. Am. Chem. Soc.* **113**, 9675 (1991).
25. Nielsen, R. P., and La Rochelle, J. H., U.S. Patent 3,962,136.
26. Emshwiller, M., Hahn, E. L., and Kaplan, D., *Phys. Rev.* **118**, 414 (1960).
27. Bassett, J., Denney, R. C., Jeffery, G. H., and Mendham, J., "Vogels Textbook of Quantitative Analysis." Longman, London, 1978.
28. Pines, A., Gibby, M. G., and Waugh, J. S., *J. Chem. Phys.* **56**, 1776 (1972).
29. Burum, D. P., and Rhim, W.-K., *J. Chem. Phys.* **71**, 944 (1979).
30. Koons, J. M., Hughes, E., and Ellis, P. D., *Anal. Chim. Acta* **283**, 1045 (1993).
31. Morè, J. J., Garbow, B. S., and Hillstrom, K. E., USDOE ANL-80-74 74 (1980).
32. Morè, J. J., *in* "Lecture Notes in Mathematics" (G. A. Watson, Ed.), Vol. 630, p. 105. Springer-Verlag, Berlin, 1977.
33. Hahn, E. L., *Phys. Rev.* **80**, 580 (1950).
34. Slichter, C. P., "Principles of Magnetic Resonance." Springer-Verlag, Berlin, 1980.
35. Wang, P. K., and Slichter, C. P., *Phys. Rev. Lett.* **53**, 82 (1984).
36. Wang, P. K., Ph.D. thesis, University of Illinois, 1984.
37. Hehre, W. J., Random, L., Schleyer, P. v. R., and Pople, J. A., "*Ab Initio* Molecular Orbital Theory," p. 167. Wiley–Interscience, New York, 1985.
38. Conroy, J., *J. Chem. Phys.* **47**, 5307 (1967).
39. Zilm, K. W., Conlin, R. T., and Grant, D. M., *J. Am. Chem. Soc.* **102**, 6672 (1980).